

This document was prepared in conjunction with work accomplished under Contract No. DE-AC09-96SR18500 with the U.S. Department of Energy.

This work was prepared under an agreement with and funded by the U.S. Government. Neither the U. S. Government or its employees, nor any of its contractors, subcontractors or their employees, makes any express or implied: 1. warranty or assumes any legal liability for the accuracy, completeness, or for the use or results of such use of any information, product, or process disclosed; or 2. representation that such use or results of such use would not infringe privately owned rights; or 3. endorsement or recommendation of any specifically identified commercial product, process, or service. Any views and opinions of authors expressed in this work do not necessarily state or reflect those of the United States Government, or its contractors, or subcontractors.

CHARACTERIZATION OF SPATIAL HETEROGENIETIES IN DETECTOR GRADE CdZnTe

M. C. Duff*, D. B. Hunter
Savannah River National Laboratory (SRNL), Aiken, SC 29808

A. Burger, M. Groza, V. Buliga
Fisk University, Nashville, TN 37208-3051

J. P. Bradley, G. Graham, Z. Dai, N. E. Teslich
Lawrence Livermore National Laboratory (LLNL), Livermore, CA 94550

D. R. Black, H. Burdette
National Inst. of Standards and Technology (NIST), Gaithersburg, MD 20899-8520

A. Lanzirotti
University of Chicago – Center for Advanced Radiation Sources (CARS), National Synchrotron Light Source, Brookhaven National Laboratory, Upton, NY 11973

* To whom correspondence should be addressed. E-mail: martine.duff@srnl.doe.gov.

Abstract

Synthetic Cd_{1-x}Zn_xTe or “CZT” crystals are highly suitable for the room temperature-based spectroscopy of gamma radiation. Structural/morphological heterogeneities within CZT, such as secondary phases that are thought to consist of Te metal and have detrimental impacts on detector performance. In this study, we used electron and X-ray-based imaging techniques to examine heterogeneous properties of detector grade CZT. Using experimental analytical techniques rather than arbitrary theoretical definitions, our study identifies two dominant secondary phase morphologies. The first consists of numerous empty, 20 μm wide, pyramidal bodies (tetrahedra) or “negative” crystals with trace quantities of particulate residue that exist as 65 nm sized particles containing Si, Cd, Zn, and Te. The other consists of 20 μm hexagonal-shaped bodies, which are composites of metallic Te layers that contain a teardrop-shaped core of amorphous and polycrystalline CdZnTe which finally surrounds an irregular-shaped void.

Introduction

Synthetic Cd_{1-x}Zn_xTe or “CZT” crystals can be used for the room temperature-based detection of γ-radiation. CZT γ-radiation detectors possess low power, small electronics packages, and they do not require cryogenic cooling—as with the commonly used germanium and silicon semiconductor detectors. Due to their modest size (a few cm³), it is possible that one could easily carry these sensitive CZT detectors and use them to quickly identify radiation γ-radiation sources. The promise of CZT for widespread use as a valuable radiation spectrometer is certainly enormous because of national security interests—regardless of country. However, research has shown that the radiation detection properties of CZT crystals can vary widely. These variances in performance are not well understood but the variances and the origins must be understood before they can be resolved. Variances have been attributed to a combination of factors ranging from point defects, structural and compositional heterogeneities within the crystals, such as twinning, pipes, grain boundaries

(polycrystallinity) and secondary phases^{1, 2, 3, 4, 5} as opposed to differences in the bulk crystallinity properties (Duff et al. 2007 and refs. therein).⁶

In the past 15 years of CZT development, as the size of useful detectors gradually increased from a few mm³ to a few cm³, the limiting factor in the detector performance seemed to vary from electron and hole trapping by point defects, pipes and cracks to what has more recently been named in the literature as either Te inclusions [as recently described by Carini et al. (2006) and refs. therein⁷ or Te precipitates.⁸ An explanation for formation of these Te-rich phases is due to the presence of excess Te in the melt of CdTe or CZT phases. Even if the starting charge is stoichiometric or slightly Cd-rich, Cd, which is the most volatile species will preferentially evaporate into the free space of the ampoule (or growth chamber) and leave behind a Te-rich melt. Tellurium-rich phases are thought to form during crystal growth or crystal cooldown due to the retrograde solubility within the phase diagram.^{9, 10 11} This was noted by Rai and researchers (1991) when they observed the presence of many <0.1 μm sized Te-rich secondary phases (called precipitates) in these materials.¹²

One of the early improvements in the CZT technology addressed the issue of the cracks and the voids within pipes. In recent years these performance limiting features have almost been eliminated from the boules grown with current methods. Fortunately, crystals made using low pressure vertical Bridgman (by Yinnel Tech in the USA)¹³ and traveling heater method [THM] (by Redlen in Canada)¹⁴ growth processes provide good control of the growth and these methods produce large single crystals by seeding or self seeding.

Poor γ -detection performance by CZT was first attributed to the presence of artifacts such as pipes and localized “Te decorations” (i.e., presumed secondary phases) at grain boundaries (Schlesinger et al. and ref. therein).¹⁵ The pipes which were readily visible by transmission IR imaging were found to be voids and the Te-rich decorations at grain boundaries were later eliminated by the use of improved growth methods.^{15, 16} As the performance of CZT for γ -ray detection improved with time, the poor performance of CZT has most recently been attributed to the presence of secondary phases (such as Te precipitates and Te inclusions) that are distributed throughout the bulk.¹⁷

While there is disagreement in the published literature emerging from crystal growth groups (as previously mentioned), a suggested terminology for the distinction between Te precipitates and Te inclusions was published by Rudolph et al. (1993;2003).^{18, 19} However the metallic nature of these presumed secondary phases of Te has not been elucidated. More importantly, the exact elemental composition of these morphological heterogeneities and the crystalline properties of them have not been directly determined for these phases. It is likely that information from these types of investigations could provide greater insight to CZT crystal growers and ultimately improve the nature of CZT for use as a radiation detector.

Several studies on CZT detector performance that measured the detector response to narrow, collimated γ -ray sources and various types of detector fabrications and geometries have attributed poor detector performance to regions of CZT (and CdTe) that are rich in secondary phases.²⁰ These and other studies concluded that these Te-rich areas limit the collection and mobility of electrons (through trapping) and that this factor strongly limits performance in those materials that are being grown with some of the current methodologies.

Some researchers have classified these perceived secondary phases as two different types of Te-rich phases that form based on processes that take place during crystal growth and cooling as discussed by Rudolf and Mühlberg.^{18, 19} The first type of these Te-rich phases is the Te inclusions, which are thought to form in melts with excess Te due to thermosolutal instabilities at the solid-liquid interface (in the absence of control over melt composition during synthesis). These phases range from 1 to several tens of μm in size and their presence in the bulk has been observed using optical microscopy. The second of these Te-rich phases (called precipitates) are thought to form during cool-down from the retrograde slope portion of the solidus. These Te precipitates are thought to be much smaller in size and range from 10 to 30 nm and can only be studied by transmission electron microscopy (TEM). Our current study presents the characterization of the morphological and elemental properties of the secondary phases in a detector grade CZT crystal.

Methods and Materials

The CZT crystals (CZT3-7-8 and CZT1b) that we examined were grown according to the Modified Vertical Bridgman (MVB) method to have $x=0.1$ Zn content as described in Li et al. (2001) and procured from Yinnel Tech (South Bend, IN). Due to the variety of experimental studies planned for the crystal called CZT3-7-8, multiple sections and sub-samples of this crystal had to be used. This single crystal (as received) was $12.4 \times 12.2 \times 15.0 \text{ mm}^3$. It was divided into three sections (CZT3-7-8-1, CZT3-7-8-2 and CZT3-7-8-3) by cutting. A $12.4 \times 12.2 \times 7 \text{ mm}^3$ portion of the crystal (CZT3-7-8-2) was polished with standard techniques down to a fine polish with $0.05\text{-}\mu\text{m}$ alumina, characterized by transmission IR imaging using a CCD camera for image recording and then prepared with gold (Au) contacts deposited by the sputtering technique. The Au contacts allowed for detector performance testing using a cesium-137 gamma source to measure (surface and bulk) resistivity and mobility-lifetime product. The high performance grade crystal called CZT1b was made into a $100 \mu\text{m}$ thin section according to Duff et al. 2007; detector performance data for this material is published elsewhere.

X-ray topography (XRT) studies were performed at the Advanced Photon Source at Argonne National Laboratory (Argonne, IL) using beam line 33-BM. An incident energy of 9 keV was selected from the white radiation source using a double crystal monochromator with Si (111) crystals. A rotating foam disc located between the sample and monochromator functioned as a random phase object to remove structure in the incident beam due to phase contrast resulting from imperfections in the beam line Be windows. The $12.4 \text{ mm} \times 12.2 \text{ mm}$ face of section CZT3-7-8-3 was parallel to (111) and symmetric (333) images were recorded from this face. The film was positioned parallel to the sample surface so that the recorded images would not have any foreshortening. Images were recorded on a high contrast lithographic film and in all images the diffraction vector points out of the image.

Reflected light optical microscopy studies were performed to examine secondary phase regions of interest on CZT3-7-8-3 using a Carl Zeiss Axio imaging system. A FEI Nova 600 Nanolab Dualbeam Focussed Ion Beam Scanning Electron Microscope (FIB-SEM) was used at 5 keV to analyze and produce thin sections of secondary phase-based areas of interest (through ion-beam milling) for high resolution-transmission electron microscopy (HR-TEM) studies. HR-TEM studies were performed with a 200 keV FEI Technai20 G2 FEG

monochromated scanning transmission electron microscope (STEM) with high angle annular dark field detector with a Si(Li) solid state X-ray detector (0.3 steradians solid angle).

Microprobe-X-ray transmission imaging studies were performed with the other detector grade CZT material (CZT1b) that was made by the same grower and method as for CZT3-7-8 (characterization, electronic and detector testing data for sample CZT1b are presented elsewhere). The X-ray transmission imaging studies were performed using a pin diode for detection of the transmitted beam at beamline X26A at the National Synchrotron Light Source (Brookhaven National Laboratory, Upton, NY). The beam size for these measurements was typically 8 by 10 microns and the X-ray energy was monochromatic (at 6-10 keV). Translation step sizes were 5 μm and count times were 10 seconds (or less) per point. Simultaneous detection of the fluorescence from the excitation of the Cd L_{3-} , Te L_{3-} and Zn K-edges using a multi-element energy-dispersive Ge detector was also possible (data not shown).

Results

Figure 1a shows a transmission IR image of CZT3-7-8-2 that reveals numerous secondary phases as indicated. There are several triangular-shaped objects in addition to objects that appear circular or more polygonal in shape. The location of a feature in the sample with respect to the position of the focal plane of the imaging system within the sample will affect the shape of the object. The resolution limit of this IR technique is $\sim 1 \mu\text{m}$, which makes detection of secondary phases of $< 1 \mu\text{m}$ not possible. There are notable differences in the size of these heterogeneities and they have a fairly random spatial distribution in the bulk. Figure 1b shows a γ -ray energy spectrum obtained for CZT3-7-8-2 demonstrating high radiation detector performance as indicated by the high-energy peak width and the limited peak tailing. This material had high surface and bulk resistivity values (ρ) of ($\rho_{\sigma} = 6.9 \times 10^{11} \Omega/\text{Sq.}$ and $\rho_{\nu} = 4.0 \times 10^{10} \Omega\text{cm}$ respectively) and a high mobility lifetime product of: $\mu\tau = 2.5 \times 10^{-3} \text{ cm}^2/\text{V}$ (data presented in Duff et al. (in review)).²¹

Several imaging methods were used to detect the presence of these secondary phases. Reflected light optical microscopy studies identified numerous triangular (pyramidal) and hexagonal regions of interest on the CZT surface as shown in Fig. 2a and 2b. Synchrotron-based microprobe X-ray transmission imaging studies with the CZT1b thin section material revealed regions of decreased atomic density or greater transmitted X-ray beam intensity as shown in Fig. 2c. Synchrotron-based X-ray fluorescence elemental imaging studies did not reveal spatial differences in the distribution of Cd, Zn or Te in the CZT although the background was sufficiently high due to the high levels of elements in this extremely pure material (data not shown). Additionally, these studies did not detect the presence of large amounts of lighter Z (contaminant or dopant) elements, which is one possible explanation for the presence of localized regions of increased X-ray transmission. Another possibility that is consistent with the results from these studies is that the sample may possess voids. Synchrotron-based XRT imaging studies (Fig. 2d) with CZT3-7-8-3 also indicate that this CZT material is heterogeneous with respect to secondary phase distribution, morphology and size. The most obvious of these features are the numerous triangular-shaped areas that appear to be consistently oriented with their vertices along (hkl) directions—see inset in Fig. 2e. One of these triangular features can be observed in Fig. 2c.

A focused ion beam-scanning electron microscope (FIB-SEM) was used to examine the surface features on both sides of CZT3-7-8-3. These examinations observed the presence of numerous empty 20- μm pyramidal bodies or “negative” crystals on both (the Cd- and Te-rich) sides of the CZT (Figs. 3a and 3b). These negative crystals were commonly observed by SEM and were oriented in a similar manner on the CZT surface. At the bottom of these voids, trace quantities of 65-nm sized particles of Si, Cd, Zn, and Te were also detected using SEM with energy dispersive X-ray spectroscopy (SEM-EDS).

In contrast to these negative crystals, several 20- μm sized hexagonal-shaped entities that are filled with metallic Te were also identified (Fig. 3c) to be present on the Te-rich face as well as the Cd-rich face. Unlike the negative crystals, these phases had a raised appearance (relative to the surface) as opposed to a depression or void. The FIB-SEM was then used to prepare thin sections for HR-TEM studies. A surface view SEM image of one of the hexagonal Te-filled bodies from the Te-rich face is shown in Fig. 3d. A platinum strap was applied to the top of the raised portion of the feature to provide stability during ion beam milling and placement on the TEM grid. Figure 3e shows an SEM image of the FIB-milled thin section after attachment of the TEM grid and prior to lifting out of the sample bulk.

HR-TEM studies were performed with the sample that was isolated from the Te-rich face as shown in Fig. 3c-d. HR-TEM images, bright field (Fig. 4a), dark field (Fig. 4b) and a composite image (Fig. 4c) of the thin section of the Te-filled feature on the CZT surface revealed various heterogeneities and features within the Te-rich secondary phases. For example, the upper portion view of the raised feature contained a faceted polycrystalline Te metal phase. This Te metal appeared to nearly encompass a relatively large body of amorphous and polycrystalline CdZnTe material. The cracks inside the Te/CdZnTe phase indicate that the entire faceted body has shrunk slightly from the rest of the host medium, which was single crystal CdZnTe. There were also small voids within the polycrystalline CdZnTe as well as within the polycrystalline Te metal.

The atomic composition of the heterogeneous Te-rich phase as determined by HR-TEM is provided in Table 1. This table reflects the levels of Cd, Zn, Te and oxygen (O) which were the primary elements detected in this sample—unlike the Si observed in the nano-crystalline particulate residue associated with the voids. Relative to the other portions of the sample (shown in Fig. 4a-c), O occurred at a level of 8.44 atom (at.)% (as determined by energy dispersive spectroscopy using the TEM) throughout the polycrystalline Te material. For comparison, the O content of the single crystal CdZnTe material was on average, 1.87 at.% and the O contents of the amorphous and polycrystalline CdZnTe were 2.18 and 1.58 at.%, respectively. Additionally, the amorphous CdZnTe was enriched in Te relative to the other phases present in the sample. The amorphous CdZnTe had about 63 at.% Te, which was 10% more Te than the bulk and polycrystalline CdZnTe, both of which had similar compositions with roughly 40% Cd, 50% Te and ~8% Zn.

On the Cd-rich face, similar voids or negative crystals and Te-rich raised features were again observed (data not shown). In most cases as visible with SEM, the Te-rich raised features exhibited cracks. These features typically had signs of surface erosion in the form of pits, which may have formed during polishing. HR-TEM analyses of a Te-rich raised feature

on the Cd-rich face revealed small voids as observed in the Te-rich sample from the Te-rich face (data not shown). The most prominent feature of the Te-rich feature from the Cd side was that it contained a high density of twin dislocations, which are a feature of plastic deformation. Grain boundaries and sub grains were easily distinguished with bright and dark field imaging as well. Again, cracks clearly separated this feature from the host single crystal CZT. Unlike the other Te, which was polycrystalline, the Te metal is crystalline. However, the crystal structure of the Te in this material could not be identified, when the selective area electron diffraction results were compared with all known data for metallic Te. Extremely low levels of trace impurity or dopant elements (molybdenum or sulfur and possibly selenium or tin) were detected in the raised features but the levels are much less than 0.0001 atom %.

Discussion

Secondary phases, often called “Te inclusions” have been defined as being 1 to 50 μm in diameter and objects of this size that are made of Te and are detectable in these crystals using transmission IR. For example, objects smaller than 1 μm have been referred to as “Te precipitates” by Rudolph and Mühlberg (1993) and in CdTe crystals these objects are in the 10 to 50 nm range which are not detectable by IR.^{18, 19} They proposed two mechanisms for Te secondary phase formation in Te-rich melts (a) during growth – as 1 to 50 μm Te inclusions and the b) formation of nm-sized Te precipitates during melt cool-down. In support of the presence of Te precipitates, HR-TEM studies with CZT grown the MVB method have recently been conducted by Wang et al. (2007).²² Wang and researchers observed the presence of nano-scale crystalline Te metal phases of less than 20 nm. The Te-rich material contained three phases of metallic Te: rhombohedral, monoclinic and hexagonal. Voids of any size domain were not noted in this study by Wang. We did not observe the presence of these nanocrystalline phases in the present study.

Our HR-TEM results indicate the possibility that more than one type of material comprises the make up of secondary phases. In some cases, voids are still present, much as was observed with the empty pipes in CZT grown using earlier growth methods but on a much smaller scale in 20 μm -sized faceted cavities.¹⁶ Using TEM techniques, Shen and colleagues (1993) investigated half empty voids that occurred within faceted secondary nano-sized phases of crystalline CdTe.⁵ Shen and colleagues (1993) proposed that the voids in these 10 to 50 nm faceted areas formed via a vacancy condensation mechanism, whereby enrichment of one type of common host atom (in this case Te) is created as the other companion atom (Cd) leaves to occupy Cd vacancies within the CdTe structure. It is conceivable that CZT may undergo similar behavior and result in vacancies as well.

We proposed that “negative” crystals or empty structures may have formed by a couple of different mechanisms. One possibility is that they form during growth by the incorporation of a gaseous bubble of Te vapor, which becomes internalized in the CZT structure. The Te may ultimately change shape from semispherical to prismatic and during crystal cool-down, the excess Te could enter the crystal bulk and leave a void. Alternatively, it is also possible that the voids form during cool-down by the condensation of Cd-vacancies. Because Cd is the most volatile species (relative to Zn and Te), it may leave the melt and occupy the gas phase above the melt. Such a process would create vacancies of Cd. At some point Cd-vacancies will condense to form the ‘negative crystal.

The cracks within the Te-rich raised features indicate a decrease in volume of the feature, which may be related to volumetric changes that occur during cool down. The voids in this particular sample are mostly associated with the polycrystalline phases. The high Te content of the amorphous CdZnTe material in the raised feature may have inhibited precipitation as a crystalline phase. However, based on our information, it is difficult to determine the various processes which have occurred that generated the heterogeneous secondary phases within this detector grade material. It is clearly apparent that within the secondary phases that we examined, there is a range of compositions, material crystallinity and phase morphologies, in addition to cracks and voids.

Finally, IR imaging which has traditionally been used to detect secondary phases in CZT is limited to the spatial detection of objects greater than 1 μm in diameter and there is limited published information about the characteristics of these micron-sized secondary phases in CZT. Our studies demonstrate that there may be a continuum of secondary phase particle sizes within CZT. Even though secondary phases ($>1 \mu\text{m}$) are known to limit local electron mobility, their presence is not sufficient to degrade bulk detector performance in some studies. However, improvements in crystal growth methods to better limit the formation of these features will hopefully yield larger volumes of high quality single crystals for use in high performance radiation detection.

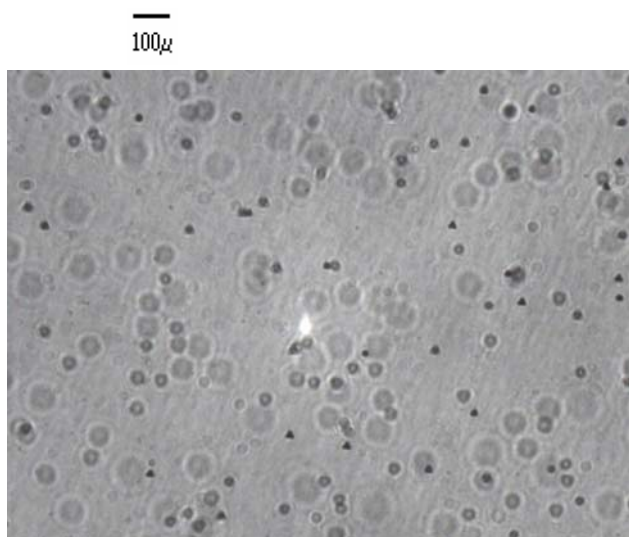
Prior to this work, the secondary phases (often called Te inclusions) that are detected through transmission-based IR imaging were thought to consist of elemental Te. Our results show that the composition and morphology of these formations are quite complex and that some of the bodies are empty. Theoretically-defined precipitates and inclusions of Te have been thought to form through different mechanisms and to have different sizes. The size of our secondary phases is consistent with that of Te inclusions. However, our conceived mechanism for their formation is more consistent with a heterogeneity that forms during cool-down, such as that for the Te "precipitates". The "negative crystals" or voids may form upon the incorporation of Te_2 gas bubbles at the melt/crystal interface and undergo vapor restructuring by developing CZT internal facets that are oriented with Te-rich side on the [111] direction of the CZT crystal. In summary, although these two morphologies have traditionally been treated as a similar crystal defect, the mechanisms for their formation (leading to practical solution for reducing their concentration) as well as their individual influence on the detector performance could be different and are yet to be fully elucidated.

Certain commercial equipment, instruments, or materials are identified in this paper in order to specify the experimental procedure adequately. Such identification is not intended to imply recommendation or endorsement by the NIST, nor is it intended to imply that the materials or equipment identified are necessarily the best available for the purpose. This work is supported by the U.S. Dept. of Energy (USDOE), Office of Nonproliferation Research and Development (NA-22). Use of the APS and the NSLS was supported by the USDOE, Office of Science, Office of Basic Energy Sciences, under Contract DE-AC02-06CH11357 and DE-AC02-98CH10886 (respectively). The authors at Fisk University gratefully acknowledge financial support from NSF for Center of Research Excellence in Science and Technology (CREST) Grant No. 0420516, and from NA-22 Grant No. DE-FG52-05NA27035.

Table 1. The atomic composition of the four phase composition types that are observed in the raised feature as image in Fig. 4a-c.

Area #	Cd (At%)	Zn (At%)	Te (At%)	O (At%)	Reference
1	42.58	7.00	48.81	1.60	EDX-5
2	42.52	6.34	49.07	2.06	EDX-1
3	42.16	6.04	49.85	1.94	EDX-8
Average	42.42	6.46	49.24	1.87	Single crystal CdZnTe
4	0.00	0.00	92.15	7.85	EDX-4
5	0.00	0.00	90.51	9.49	EDX-2
6	0.00	0.00	92.00	8.00	EDX-3
7	0.00	0.00	90.90	9.10	EDX-6
8	0.00	0.00	93.05	6.95	EDX-7
9	0.00	0.00	90.74	9.26	EDX-16
Average	0.00	0.00	91.56	8.44	Polycrystalline Te
10	32.59	5.10	61.15	1.14	EDX-13
11	32.86	4.40	59.84	2.91	EDX-11
12	24.38	3.61	69.35	2.65	EDX-18
13	30.30	4.05	63.64	2.01	EDX-15
Average	30.03	4.29	63.49	2.18	Amorphous CdZnTe
14	40.45	5.22	53.18	1.14	EDX-10
15	41.68	5.02	51.67	1.63	EDX-12
16	40.04	5.46	52.06	2.44	EDX-9
17	41.29	5.61	51.98	1.12	EDX-14
Average	40.86	5.33	52.22	1.58	Polycrystalline CdZnTe

a)



b)

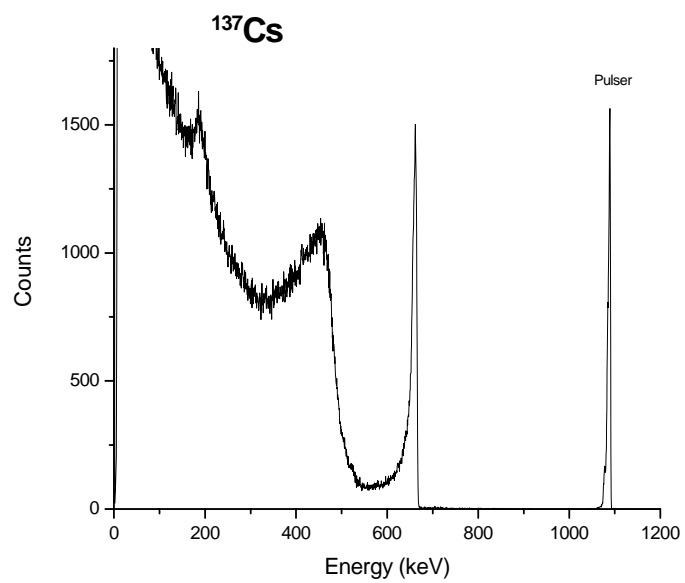


Figure 1. Characterization and testing of CZT-3-7-8. a) transmission IR image (Area: 1.5 x 2.0 mm²; depth of field is 0.25 mm , b) γ -ray measurement using Cs-137 (bias: 1000V; FWHM: 1.7%)

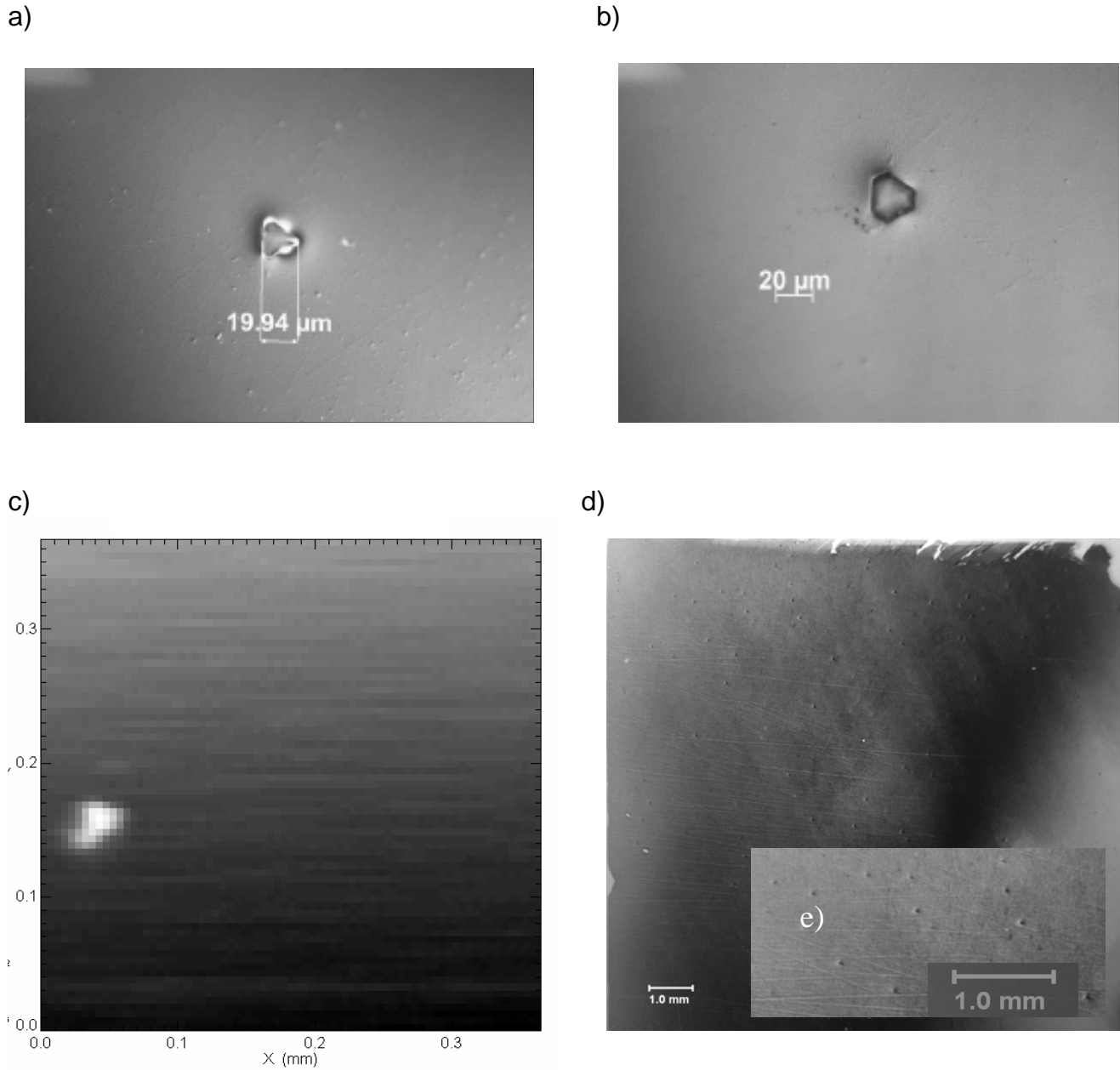


Figure 2. Optical microscopy images of a) a pyramidal feature, and b) a faceted feature and c) a transmission-based X-ray image of another high detector performance CZT thin section (also made using the MVB) method where lighter regions indicate greater beam transmission through the thin section sample; d) X-ray topograph with e) (inset) a close-up of heterogeneous pyramidal feature as shown as an enlargement of d).

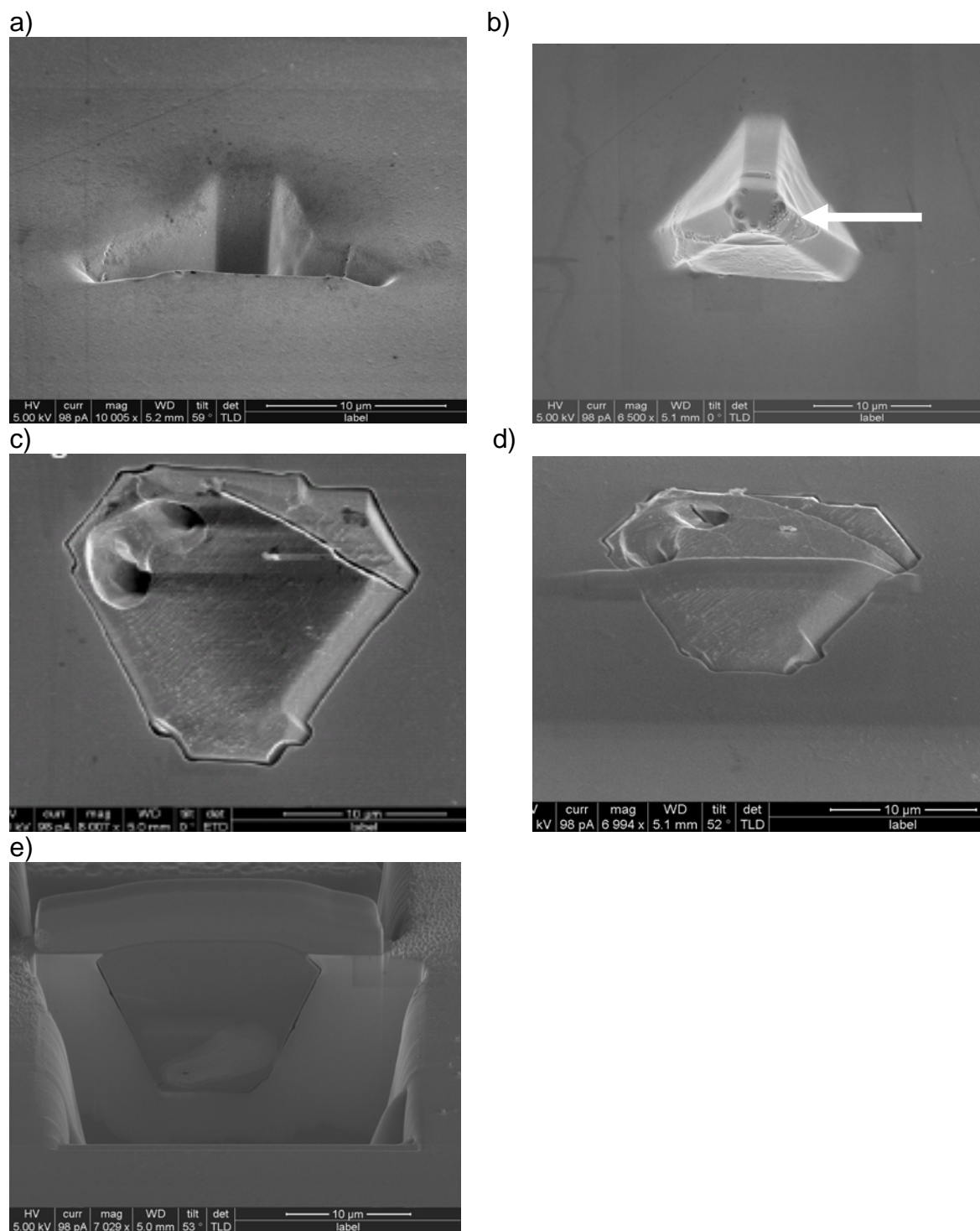


Figure 3. SEM image: a) voids (negative crystals) in CZT; view from 68° tilt and b) overhead view from 0° tilt from surface normal c) raised feature (from 0° tilt from surface) containing Te metal d) and e) with FIB preparation of cross section of raised feature for TEM imaging with Pt strap and C coating. Arrow in 3b shows particulate residue at bottom of negative crystal that contains 65-nm sized particles of Si, Cd, Zn, and Te.

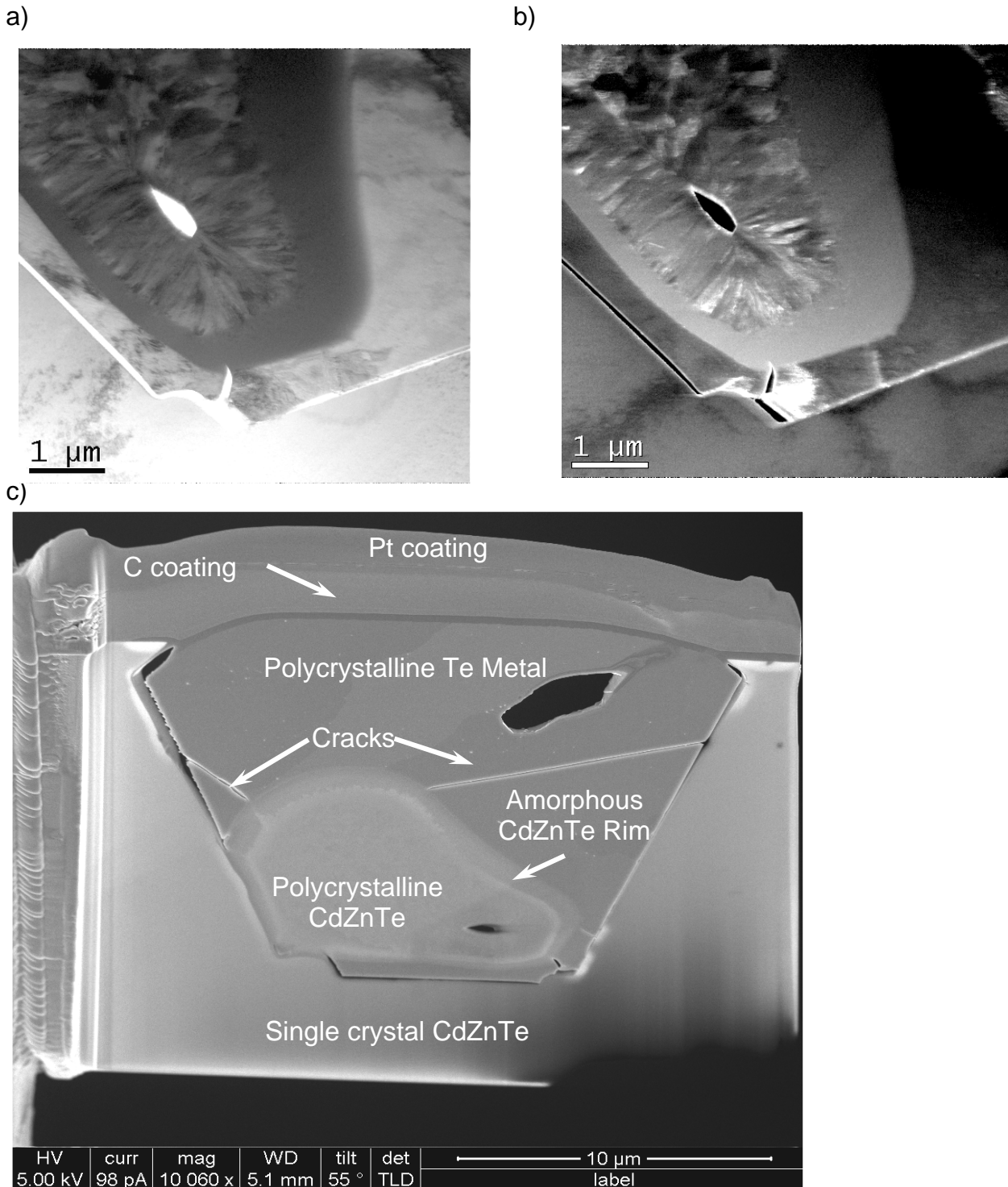


Figure 4. HR-TEM images of thin section of Te-filled raised feature on CZT surface showing a) bright and b) dark field imaging and c) resulting composite of TEM imaging analyses with delineation of four various heterogeneities in the Te-rich secondary phases.

References

- ¹ J. R. Heffelfinger, D. L. Medlin, R. B. James. *MRS Symp. Ser.* 487:33-38 (1998).
- ² M. Schieber, T. E. Schlesinger, R. B. James, H. Hermon, H. Yoon, M. Goorsky. *J. Crystal Growth* 237-239:2082-2090 (2002).
- ³ C. Szeles, M. C. Driver. *SPIE Proc.* 3446:1-8 (1998).
- ⁴ C. Szeles, S. E. Cameron, J-O. Ndap, W. C. Chalmers. *IEEE Trans. Nuclear Sci.* 49:2535-2540 (2002).
- ⁵ J. Shen, D. K. Aidun, L. Regel, W. R. Wilcox. *J. Crystal Growth* 132:250-260 (1993).
- ⁶ M. C. Duff, D. B. Hunter, P. Nuessle, D. R. Black, H. Burdette, J. Woicik, A. Burger, M. Groza. *J. Electronic Materials.* 36:1092-1097 (2007).
- ⁷ G. A. Carini, A. E. Bolotnikov, G. S. Camarda, G. W. Wright, L. Li, R. B. James. *Appl. Physics Lett.* 88:143515 (2006).
- ⁸ C. Szeles, W. C. Chalmers, S. C. Cameron, J-O. Ndap, M. Bliss, K. G. Lynn. *SPIE Proc.* 4507:57-67 (2001).
- ⁹ P. Rudolph, M. Neubert, M. Mühlberg. *J. Crystal Growth.* 128:582-587 (1993).
- ¹⁰ P. Rudolph, A. Engel, I. Schentke, A. Grochochi. *J. Crystal Growth.* 147:297-304 (1995).
- ¹¹ J. L. Pautrat, M. Magnea, J. P. Faurie, *J. Appl. Phys.* 53:8668-8677 (1982).
- ¹² R. S. Rai, S. Mahajan, S. McDevitt, C. J. Johnson. *J. Vacuum. Sci. Technol.* B9:1892-1996.
- ¹³ L. Li, F. Lu, K. Shah, M. Squillante, L. Cirinano, W. Yao, R. W. Olson, P. Luke, Y. Nemirovsky, A. Burger, G. Wright, R. B. James. *Nuclear Sci. Symp. Conf. Rec. IEEE* 4:2396-2400 (2001).
- ¹⁴ H. Chen, S. A. Awadalla, R. Redden, G. Brindley, A. Copete, J. Hong, H. Grindlay, M. Amman, J. S. Lee, P. Luke. *IEEE Trans. Nuclear Sci.* 6: 3809-3816 (2007).
- ¹⁵ T. E. Schlesinger, J. E. Toney, H. Yoon, E. Y. Lee, B. A. Brunett, L. Franks, R. B. James. *Material Sci. Engineering.* 32:103-189 (2001).
- ¹⁶ C. Szeles, E. E. Eissler. *MRS Symp. Series* 487:3-12 (1998).
- ¹⁷ P. N. Luke, M. Amman, J. S. Lee. *IEEE Trans. Nuclear Sci.* 51:1199-1203 (2004).
- ¹⁸ P. Rudolph, M. Mühlberg. *Material Sci. Engineering.* B16:8-16 (1993).
- ¹⁹ P. Rudolph. *Crystal Res. Technol.* 38:542-554 (2003).
- ²⁰ B. H. Parker, C. M. Stahle, S. D. Barthelmy, A. M. Parsons, J. Tueller, J. T. Van Sant, B. F. Munoz, S. J. Snodgrass, R.E. Mullinix. *SPIE* 3768:129-137 (1999).

²¹ M. C. Duff, D. B. Hunter, A. Burger, M. Groza, V. Buliga, D. R. Black. *Appl. Surf. Sci.* in press (2007).

²² T. Wang, W. Jie, D. Zeng. *Material Sci. Engineering.* (2007) in press. Available online 3/19/07.